Chapter 6

Experiments with annuli of variable depth.

Measurements with a flat base, and both insulating and conducting barriers have shown that the η and ζ-circulations play significant roles in heat advection in fully blocked annulus systems. However the role of the eddies which appear at higher values of Ω has not been determined.

This chapter aims to test the hypothesis that heat advection by eddies accounts for the difference between the measurements of heat advection, and the heat advection calculated for the η and ζ-circulations. If this is the case, then in a system where no eddies occur, the measured heat advection should be the same as that calculated for the η and ζ-circulations.

The experiments described in this chapter used fully blocking insulating barriers with two types of sloping bases. Previous work (*Hide and Mason (1975), Mason (1972), (1975)* and *Hide (1969)*) has shown that sloping bases can be effective in suppressing the formation of waves in unblocked annulus experiments. Increasing Ω tends to constrain fluid particles to move on surfaces parallel to the lid and base of the apparatus, as *Mason (1975)* puts it,

> 'At more rapid rotation rates the vertical stiffness of the fluid increases and the presence of the boundaries is felt throughout the interior of the fluid (cf. the Taylor-Proudman theorem (Greenspan 1968)).'

Only fluid trajectories at certain quite well defined angles to the geopotentials in the fluid can release energy by sloping convection. Thus a base which constrains fluid particles to move at angles (as above) other than those which can release energy through sloping convection can prevent it from occurring. Similarly a different choice of sloping base can encourage fluid particles to move at an angle appropriate for energy release by sloping convection, and thus stimulate it.

In general fluid trajectories which make an angle to the geopotential surfaces in the fluid, which is less than the angle to the geopotentials made by the isotherms, may release energy by sloping convection. In practice the experimental technique seems to be to choose sloping bases which make about the same angle to the geopotentials as the isotherms. Bases which slope in the same sense as the isotherms tend to stabilize the flow at low Ω and destabilize it at high Ω, unless the slopes are very steep, in which case they always stabilize the flow. Bases which slope in the opposite sense to the isotherms tend to destabilize the flow at low Ω, but to stabilize it at high Ω. Further details about the effect of sloping bases on baroclinic instability should be sought in *Mason (1975)*.

The bases chosen for the measurements made in this chapter were designed by D.W.Johnson, they sloped in the opposite sense to the isotherms. This was because the waves seen in the full thermally insulating barrier experiments (chapter 3) were quite weak, and it was felt that either suppressing or stimulating the waves could lead to some interesting results. However it is perhaps worth observing that since the transition for the onset of the waves occurred at much higher Ω than for an unobstructed annulus (see *Figure 3.1*), such a choice might be regarded as being more likely to stabilize the flow in any event, because such a base exerts a stabilizing influence at high Ω.

If β is the angle of an isotherm to a geopotential, then neglecting the centrifu-

gal force,

$$\tan\beta \approx \left(\frac{\partial T}{\partial x}\right)\left(\frac{\partial T}{\partial z}\right)^{-1} \approx \frac{\Delta T_H d}{\Delta T_z \Delta x}.$$

Where x is some horizontal coordinate, Δx some horizontal length scale and ΔT_H is the appropriate horizontal temperature difference in the body of the fluid. The last term has been derived by assuming linear temperature gradients in the fluid. For the full barrier results in chapter 3, a suitable estimate for the maximum azimuthal slope of the isotherms can be made by putting $\Delta T_H = \Delta T_\phi \approx 0.25\Delta T$, $\Delta T_z \approx \Delta T$, and $\Delta x \approx 2\pi\bar{r}$. This gives an azimuthal slope, $\beta_\phi \approx 6°$ at $r = \bar{r}$. For the radial slope, generally $\partial T/\partial r$ was very small, with $\Delta T_r \approx 0.05\Delta T$ (with $\Delta x \approx 3.5cm$) at small Ω or across the sides of the interior of the fluid at high Ω (see *Figure 1.4(b)*). However at high Ω, in the body of the fluid, ΔT_r reached about $0.10\Delta T$ over a distance of $\Delta x \approx 2cm$. These values gave the radial slope of the isotherms to be between 11° and 35°.

On the basis of this information, the following slopes were chosen for the two bases; (i) a slope of 6° in azimuth ($r = \bar{r}$), with no radial slope for the base where $d = d(\phi)$, and (ii) a slope of 24° with radius (mid-range between 11° and 35°), and 2° with azimuth ($r = \bar{r}$) for the $d = d(r, \phi)$ base. The small azimuthal slope for the $d(r, \phi)$ base prevents its highest part from interfering with the thermocouple ring which was at mid-depth. However it must be stressed that the effect of any given sloping base on the flow is very much a matter of trial and error.

The two sloping bases used are shown in *Figure 2.2* and described in more detail in §2.1.1. Following the notation above, the base described in §2.1.1 (experimental configuration number 3) and shown in *Figure 2.2 (c)* shall be referred to as the $d(\phi)$ base, and the base described in §2.1.1 (experimental configuration number 4) and shown in *Figure 2.2 (d)* shall be referred to as the $d(r, \phi)$ base. The reader is strongly recommended to turn to *Figure 2.2* (on page 38) to refresh their memory as to the form of these two bases.

The results are given in §6.1; §6.1.1 deals with the system with $d(\phi)$, §6.1.2 the system with $d(r, \phi)$. The results are discussed in §6.2, the η-circulation in §6.2.1 and the ζ-circulation in §6.2.2. The role of eddies is considered in §6.2.3. The conclusions drawn from these experiments are given in §6.3.

6.1 Temperature measurements.

6.1.1 System with variable depth, $d(\phi)$.

A regime diagram showing the values of Θ and τ for all the temperature and heat transport measurements made with the system with an insulating barrier and variable depth, $d(\phi)$ is shown in *Figure 6.1*. Comparison with *Figure 3.8* shows that the sloping base has stabilized the flow so that eddies form when $\Theta \lesssim 0.2 - 0.03$ and $\tau \gtrsim 2 \times 10^7 - 1 \times 10^8$ (compared with $\Theta \lesssim 0.5 - 0.1$ and $\tau \gtrsim 10^7$ with a flat base).

Figure 6.2 shows the fluid temperature measured by the thermocouple ring at $z = 0$ and $r = \bar{r}$, $T(\bar{r}, z = 0; \phi, t)$. The barrier is placed at the centre of the diagram. The results are quite similar to those of *Figure 3.9*, (a) shows the 'kinks' associated with higher rotation rates.

The increase in ΔT_B with Ω can be seen in *Figure 6.3*. While ΔT_B increases linearly with Ω before levelling off, it rises more quickly and reaches a value of $\sim 40\%$ of ΔT, a larger value than either the insulating or conducting barrier experiments.

Figure 6.4 shows the dependence of Nusselt number on Ω. The heat transport results are quite similar to those with a flat base, though the heat transport tends to be a little less.

The temperature and heat transport measurements are summarized in *Tables 6.1* and *6.2*.

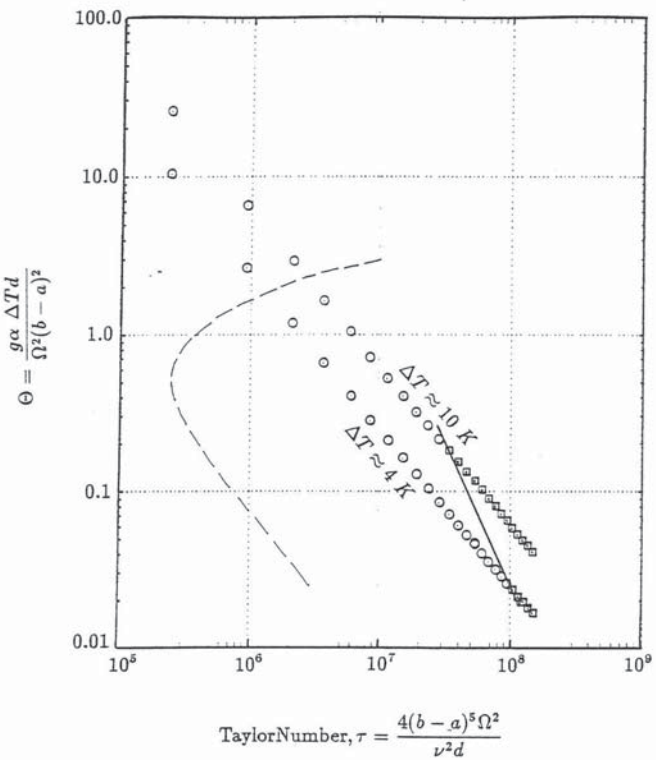

FIGURE 6.1: Regime diagram showing the values of τ and Θ for runs 282-336, the experiments with a full insulating radial barrier, and variable depth, $d(\phi)$. The circles show results where temperature measurements indicated there were no eddies in the system, and the squares show measurements where small eddies were present. The dashed line indicates the approximate location of the transition for the onset of baroclinic waves in an unblocked annulus, such as that used by *Fowlis and Hide (1965)*. The location of the dashed line was obtained from D.W.Johnson (private communication), while the solid line indicates the transition for the onset of eddies in the present experiments.

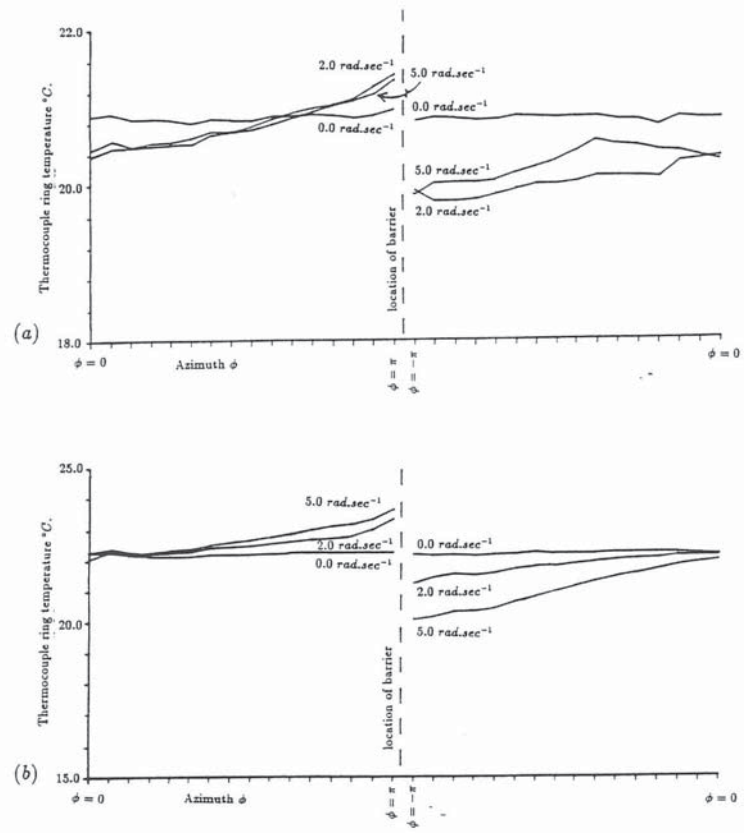

FIGURE 6.2: Measurements showing the temperature of ring thermocouple against ϕ for $\Omega = 0.0, 2.0$ and $5.0\ rad.sec^{-1}$, for the system with $d(\phi)$. Each of the scale markings along the horizontal axis shows the location of one of the thermocouples in the ring. A straight line is drawn between each point to serve as a guide for the eye. The location of the barrier is shown by the vertical dashed line. The standard errors were (a) $0.008°C$, and (b) $0.016°C$. For (a) $\Delta T \approx 4\ K$ and (b) $\Delta T \approx 10\ K$. Note that ΔT_B was defined as the difference between the maximum and minimum thermocouple ring temperatures. As the figures show these were usually at or near the sides of the barrier.

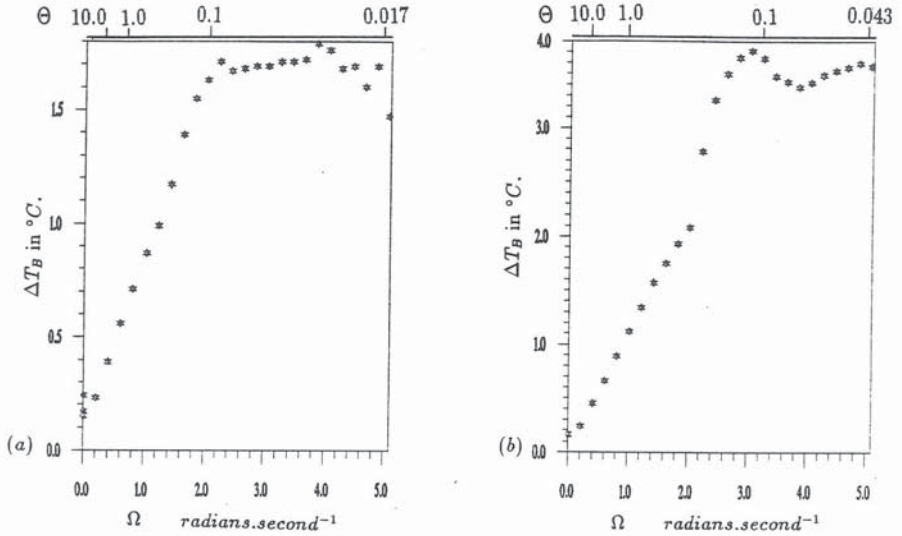

FIGURE 6.3: Measurements showing the dependence of ΔT_B on Ω for the system with $d(\phi)$. (a) $\Delta T \approx 4\ K$, (b) $\Delta T \approx 10\ K$.

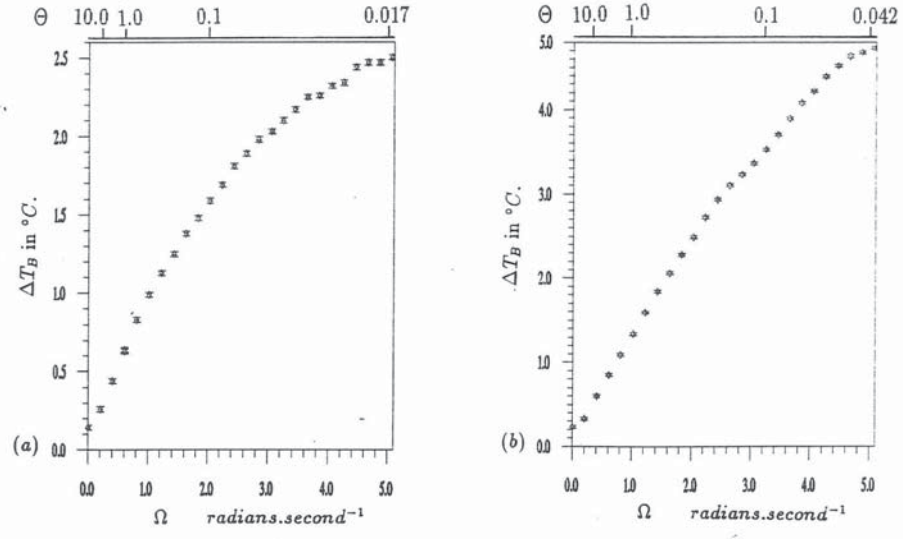

FIGURE 6.7: Measurements showing the dependence of ΔT_B on Ω for the system with $d(r, \phi)$. (a) $\Delta T \approx 4\ K$, (b) $\Delta T \approx 10\ K$.

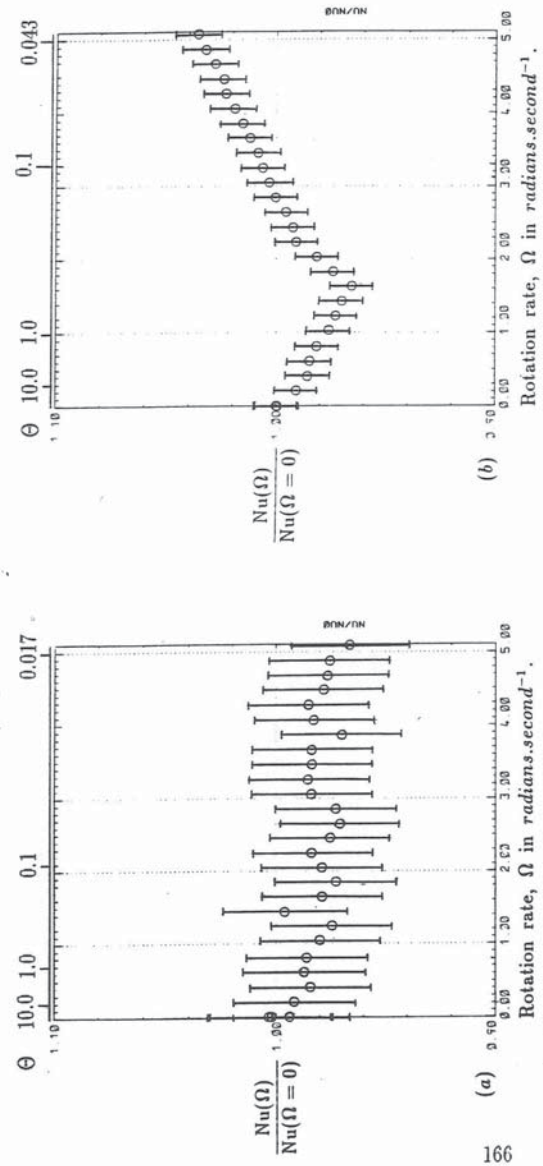

FIGURE 6.4: Measurements showing the dependence of Nusselt number, $Nu(\Omega)$, divided by $Nu(\Omega = 0)$, on Ω, for the system with $d(\phi)$. (a) $\Delta T \approx 4\ K$, (b) $\Delta T \approx 10\ K$.

TABLE 6.1: Temperature and heat transport measurements for the annulus with a sloping base, $d(\phi)$.

Run No	ΔT K	Ω $rad.sec^{-1}$	ΔT_{BAR} K	Prandtl No	Θ	Taylor No	Rayleigh No	Ekman No	$H_{conductive}$ $watts$	H_{total} $watts$	Nusselt No
282	3.95	0.000	0.24	14.14	∞	0	8.38×10^6	∞	1.21	13.28	11.01
283	4.01	0.000	0.17	14.14	∞	0	8.50×10^6	∞	1.22	13.58	11.11
284	4.02	0.203	0.23	14.14	1.04×10^1	2.32×10^5	8.52×10^6	1.48×10^{-3}	1.23	13.46	10.98
285	4.03	0.404	0.39	14.14	2.64	9.16×10^5	8.53×10^6	7.42×10^{-4}	1.23	13.38	10.90
286	4.03	0.000	0.15	14.14	∞	0	8.54×10^6	∞	1.23	13.64	11.10
287	4.00	0.605	0.56	14.14	1.17	2.05×10^6	8.48×10^6	4.96×10^{-4}	1.22	13.33	10.93
288	4.00	0.806	0.71	14.14	6.59×10^{-1}	3.64×10^6	8.48×10^6	3.72×10^{-4}	1.22	13.33	10.92
289	4.01	1.032	0.87	14.14	4.03×10^{-1}	5.97×10^6	8.50×10^6	2.91×10^{-4}	1.22	13.27	10.85
290	4.01	1.234	0.99	14.14	2.82×10^{-1}	8.53×10^6	8.49×10^6	2.43×10^{-4}	1.22	13.17	10.79
291	4.02	1.436	1.17	14.14	2.09×10^{-1}	1.16×10^7	8.52×10^6	2.09×10^{-4}	1.23	13.51	11.03
292	4.02	1.638	1.39	14.14	1.60×10^{-1}	1.50×10^7	8.52×10^6	1.83×10^{-4}	1.22	13.28	10.84
293	4.02	1.839	1.55	14.14	1.27×10^{-1}	1.90×10^7	8.52×10^6	1.63×10^{-4}	1.23	13.19	10.77
294	4.00	2.041	1.63	14.14	1.03×10^{-1}	2.33×10^7	8.48×10^6	1.47×10^{-4}	1.22	13.23	10.84
295	4.01	2.243	1.71	14.14	8.53×10^{-2}	2.82×10^7	8.50×10^6	1.34×10^{-4}	1.22	13.31	10.89
296	4.01	2.445	1.67	14.14	7.18×10^{-2}	3.35×10^7	8.50×10^6	1.23×10^{-4}	1.22	13.20	10.80
297	4.01	2.647	1.68	14.14	6.12×10^{-2}	3.93×10^7	8.49×10^6	1.13×10^{-4}	1.22	13.13	10.75
298	4.00	2.849	1.69	14.14	5.26×10^{-2}	4.55×10^7	8.47×10^6	1.05×10^{-4}	1.22	13.12	10.77
299	3.99	3.050	1.69	14.14	4.59×10^{-2}	5.21×10^7	8.45×10^6	9.84×10^{-5}	1.22	13.24	10.89
300	3.99	3.252	1.71	14.14	4.04×10^{-2}	5.93×10^7	8.46×10^6	9.23×10^{-5}	1.22	13.28	10.91
301	3.98	3.453	1.71	14.14	3.57×10^{-2}	6.68×10^7	8.44×10^6	8.69×10^{-5}	1.21	13.23	10.89
302	3.98	3.656	1.72	14.14	3.18×10^{-2}	7.49×10^7	8.42×10^6	8.21×10^{-5}	1.21	13.19	10.89
303	3.99	3.861	1.79	14.14	2.87×10^{-2}	8.35×10^7	8.46×10^6	7.77×10^{-5}	1.22	13.07	10.74
304	3.98	4.064	1.76	14.14	2.58×10^{-2}	9.25×10^7	8.44×10^6	7.38×10^{-5}	1.21	13.22	10.88
305	4.00	4.266	1.68	14.14	2.35×10^{-2}	1.02×10^8	8.47×10^6	7.03×10^{-5}	1.22	13.29	10.91
306	3.99	4.467	1.69	14.14	2.14×10^{-2}	1.12×10^8	8.46×10^6	6.72×10^{-5}	1.22	13.18	10.83
307	3.99	4.671	1.60	14.14	1.96×10^{-2}	1.22×10^8	8.46×10^6	6.42×10^{-5}	1.22	13.15	10.81
308	4.00	4.872	1.69	14.14	1.80×10^{-2}	1.33×10^8	8.47×10^6	6.16×10^{-5}	1.22	13.16	10.80
309	3.99	5.076	1.47	14.14	1.66×10^{-2}	1.44×10^8	8.46×10^6	5.91×10^{-5}	1.22	13.01	10.70

TABLE 6.2: Temperature and heat transport measurements for the annulus with a sloping base, $d(\phi)$.

Run No	ΔT K	Ω $rad.sec^{-1}$	ΔT_{BAR} K	Prandtl No	Θ	Taylor No	Rayleigh No	Ekman No	$H_{conductive}$ $watts$	H_{total} $watts$	Nusselt No
310	10.01	0.000	0.16	14.14	∞	0	2.12×10^7	∞	3.05	45.51	14.92
311	10.01	0.000	0.16	14.14	∞	0	2.12×10^7	∞	3.05	45.49	14.91
312	10.01	0.204	0.24	14.14	2.57×10^1	2.34×10^5	2.12×10^7	1.47×10^{-3}	3.05	45.10	14.78
313	10.00	0.406	0.45	14.14	6.50	9.22×10^5	2.12×10^7	7.40×10^{-4}	3.05	44.81	14.70
314	10.00	0.607	0.66	14.14	2.90	2.07×10^6	2.12×10^7	4.94×10^{-4}	3.05	44.78	14.69
315	10.01	0.808	0.89	14.14	1.64	3.66×10^6	2.12×10^7	3.71×10^{-4}	3.05	44.65	14.64
316	10.00	1.020	1.12	14.14	1.03	5.84×10^6	2.12×10^7	2.94×10^{-4}	3.05	44.39	14.56
317	10.00	1.223	1.34	14.14	7.16×10^{-1}	8.38×10^6	2.12×10^7	2.45×10^{-4}	3.05	44.25	14.51
318	10.00	1.425	1.57	14.14	5.27×10^{-1}	1.14×10^7	2.12×10^7	2.11×10^{-4}	3.05	44.11	14.47
319	10.01	1.629	1.75	14.14	4.03×10^{-1}	1.49×10^7	2.12×10^7	1.84×10^{-4}	3.05	43.92	14.40
320	10.00	1.829	1.93	14.14	3.20×10^{-1}	1.87×10^7	2.12×10^7	1.64×10^{-4}	3.05	44.30	14.53
321	9.99	2.030	2.08	14.14	2.59×10^{-1}	2.31×10^7	2.12×10^7	1.48×10^{-4}	3.05	44.61	14.64
322	9.99	2.232	2.78	14.14	2.14×10^{-1}	2.79×10^7	2.12×10^7	1.34×10^{-4}	3.05	45.02	14.78
323	9.98	2.434	3.26	14.14	1.80×10^{-1}	3.32×10^7	2.11×10^7	1.23×10^{-4}	3.04	45.03	14.80
324	9.98	2.636	3.50	14.14	1.54×10^{-1}	3.89×10^7	2.11×10^7	1.14×10^{-4}	3.04	45.17	14.85
325	9.98	2.837	3.65	14.14	1.33×10^{-1}	4.51×10^7	2.11×10^7	1.06×10^{-4}	3.04	45.36	14.92
326	9.96	3.039	3.71	14.14	1.15×10^{-1}	5.17×10^7	2.11×10^7	9.87×10^{-5}	3.04	45.45	14.96
327	9.97	3.241	3.64	14.14	1.02×10^{-1}	5.89×10^7	2.11×10^7	9.26×10^{-5}	3.04	45.60	15.01
328	9.96	3.443	3.48	14.14	8.99×10^{-2}	6.64×10^7	2.11×10^7	8.71×10^{-5}	3.04	45.67	15.04
329	9.96	3.645	3.43	14.14	8.02×10^{-2}	7.45×10^7	2.11×10^7	8.23×10^{-5}	3.04	45.86	15.10
330	9.98	3.848	3.38	14.14	7.21×10^{-2}	8.30×10^7	2.11×10^7	7.80×10^{-5}	3.04	46.07	15.15
331	9.97	4.048	3.42	14.14	6.51×10^{-2}	9.18×10^7	2.11×10^7	7.41×10^{-5}	3.04	46.22	15.21
332	9.97	4.250	3.49	14.14	5.91×10^{-2}	1.01×10^8	2.11×10^7	7.06×10^{-5}	3.04	46.39	15.26
333	9.98	4.454	3.53	14.14	5.38×10^{-2}	1.11×10^8	2.11×10^7	6.74×10^{-5}	3.04	46.45	15.28
334	9.96	4.655	3.56	14.14	4.92×10^{-2}	1.21×10^8	2.11×10^7	6.45×10^{-5}	3.04	46.55	15.33
335	9.96	4.858	3.60	14.14	4.51×10^{-2}	1.32×10^8	2.11×10^7	6.18×10^{-5}	3.04	46.75	15.40
336	9.95	5.060	3.57	14.14	4.16×10^{-2}	1.44×10^8	2.11×10^7	5.93×10^{-5}	3.03	46.89	15.45

6.1.2 System with variable depth, $d(r, \phi)$.

The regime diagram for the measurements made with a system with variable depth, $d(r, \phi)$ is shown in *Figure 6.5*. For $\Delta T \approx 4\ K$ the sloping base prevented the formation of eddies over the entire range of parameters used ($1.64 \times 10^{-2} < \Theta < \infty$ and $0 < \tau < 1.46 \times 10^{8}$). When $\Delta T \approx 10\ K$ eddies formed for $\Theta \lesssim 0.15$ and $\tau \gtrsim 3 \times 10^{7}$.

Figure 6.6 shows the fluid temperature measured by the thermocouple ring, $T(\bar{r}, z = 0; \phi, t)$. The barrier is placed at the centre of the diagram. Generally these results look less linear than with the insulating barrier, but the 'kinks' appear most strongly at higher Ω.

ΔT_B is plotted against Ω in *Figure 6.7*. While ΔT_B still increases with Ω before tending to level off, its behaviour now looks less linear, and ΔT_B levels off more gradually. ΔT_B reaches a maximum value of $\sim 50 - 60\%$ of ΔT, a higher value than seen in any other of the full radial barrier experiments.

The heat transport results are shown in *Figure 6.8*. When $\Delta T \approx 4\ K$ the Nusselt number decreases significantly with Ω, a result not seen in any of the other full radial barrier experiments. When $\Delta T \approx 10\ K$ the Nusselt number decreases with Ω but the effect is not nearly so marked.

The temperature and heat transport measurements are summarized in *Tables 6.3* and *6.4*.

6.1.3 Summary of results.

Both the sloping bases types inhibited the formation of eddies to some extent. Comparison of *Figures 6.1* and *6.5* shows that the system with a base that caused the depth to vary with both r and ϕ inhibited the formation of eddies slightly more than the system where the depth varied with ϕ only.

The sloping bases affected ΔT_B, increasing it above the values seen with either

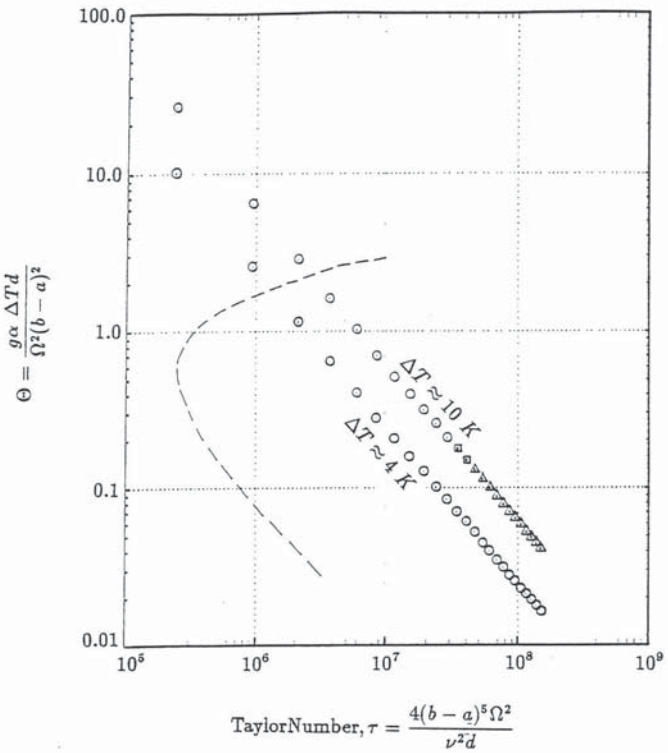

FIGURE 6.5: Regime diagram showing the values of τ and Θ for runs 337-391, the experiments with a full insulating radial barrier, and variable depth, $d(r, \phi)$. The circles show results where temperature measurements indicated there were no eddies in the system, the triangles show measurements where eddies were present, and the squares show measurements where it was difficult to tell whether eddies were present or not. The dashed line indicates the approximate location of the transition for the onset of baroclinic waves in an unblocked annulus, such as that used by *Fowlis and Hide (1965)*. The location of the dashed line was obtained from D.W.Johnson (private communication), while the solid line indicates the location of the transition for the onset of eddies in the present experiments.

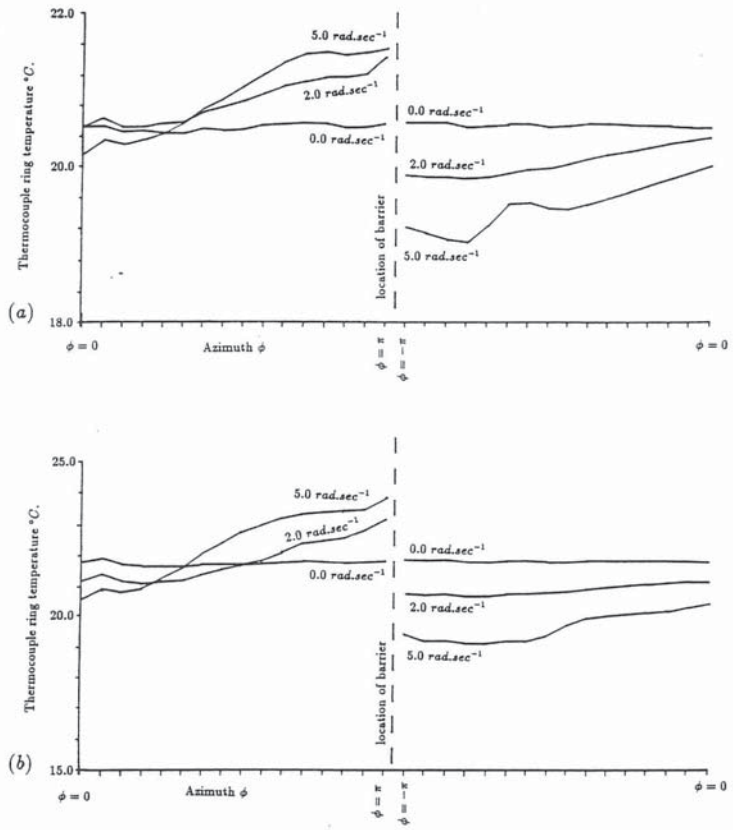

FIGURE 6.6: Measurements showing the temperature of ring thermocouple against ϕ for $\Omega = 0.0, 2.0$ and $5.0\ rad.sec^{-1}$, for the system with $d(r, \phi)$. Each of the scale markings along the horizontal axis shows the location of one of the thermocouples in the ring. A straight line is drawn between each point to serve as a guide for the eye. The location of the barrier is shown by the vertical dashed line. The standard errors were $0.016°C$. For (a) $\Delta T \approx 4\ K$ and (b) $\Delta T \approx 10\ K$. Note that ΔT_B was defined as the difference between the maximum and minimum thermocouple ring temperatures. As the figures show these were usually at or near the sides of the barrier.

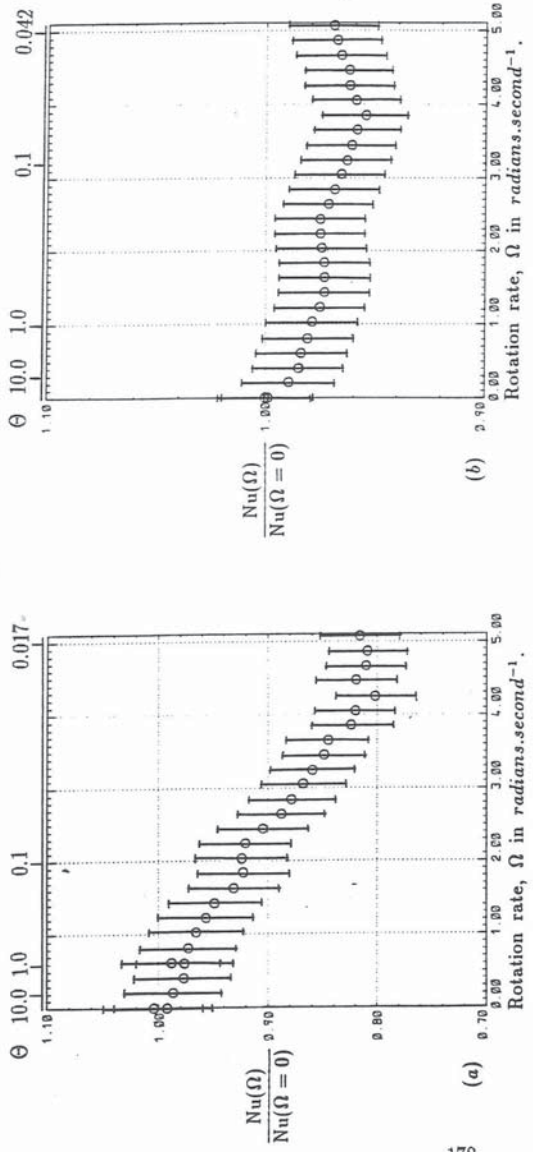

FIGURE 6.8: Measurements showing the dependence of Nusselt number, $Nu(\Omega)$, divided by $Nu(\Omega = 0)$, on Ω, for the system with $d(r, \phi)$. (a) $\Delta T \approx 4\ K$, (b) $\Delta T \approx 10\ K$.

TABLE 6.3: Temperature and heat transport measurements for the annulus with a sloping base, $d(r,\phi)$.

Run No	ΔT K	Ω $rad.sec^{-1}$	ΔT_{BAR} K	Prandtl No	Θ	Taylor No	Rayleigh No	Ekman No	$H_{conductive}$ $watts$	H_{total} $watts$	Nusselt No
337	4.00	0.000	0.14	14.14	∞	0	8.48×10^{6}	∞	1.20	13.63	11.39
338	4.00	0.000	0.14	14.14	∞	0	8.47×10^{6}	∞	1.20	13.49	11.29
339	4.00	0.202	0.26	14.14	1.02×10^{1}	2.34×10^{5}	8.47×10^{6}	1.48×10^{-3}	1.20	13.39	11.19
340	4.00	0.404	0.44	14.14	2.58	9.30×10^{5}	8.47×10^{6}	7.43×10^{-4}	1.20	13.26	11.09
341	4.00	0.605	0.64	14.14	1.15	2.09×10^{6}	8.48×10^{6}	4.96×10^{-4}	1.20	13.25	11.07
342	3.99	0.605	0.63	14.14	1.14	2.09×10^{6}	8.45×10^{6}	4.96×10^{-4}	1.19	13.36	11.20
343	3.99	0.806	0.83	14.14	6.44×10^{-1}	3.71×10^{6}	8.45×10^{6}	3.72×10^{-4}	1.19	13.15	11.03
344	3.99	1.020	0.99	14.14	4.03×10^{-1}	5.94×10^{6}	8.46×10^{6}	2.94×10^{-4}	1.19	13.08	10.95
345	4.01	1.222	1.13	14.14	2.82×10^{-1}	8.53×10^{6}	8.49×10^{6}	2.46×10^{-4}	1.20	13.01	10.85
346	3.99	1.424	1.25	14.14	2.07×10^{-1}	1.16×10^{7}	8.46×10^{6}	2.11×10^{-4}	1.19	12.85	10.76
347	4.01	1.626	1.38	14.14	1.59×10^{-1}	1.51×10^{7}	8.49×10^{6}	1.85×10^{-4}	1.20	12.66	10.56
348	4.01	1.827	1.48	14.14	1.26×10^{-1}	1.91×10^{7}	8.49×10^{6}	1.64×10^{-4}	1.20	12.54	10.46
349	4.01	2.029	1.59	14.14	1.02×10^{-1}	2.35×10^{7}	8.49×10^{6}	1.48×10^{-4}	1.20	12.57	10.48
350	3.98	2.230	1.69	14.14	8.41×10^{-2}	2.84×10^{7}	8.44×10^{6}	1.35×10^{-4}	1.19	12.45	10.44
351	3.99	2.433	1.81	14.14	7.07×10^{-2}	3.38×10^{7}	8.45×10^{6}	1.23×10^{-4}	1.19	12.24	10.26
352	4.00	2.636	1.89	14.14	6.05×10^{-2}	3.97×10^{7}	8.48×10^{6}	1.14×10^{-4}	1.20	12.06	10.07
353	3.99	2.837	1.98	14.14	5.20×10^{-2}	4.59×10^{7}	8.45×10^{6}	1.06×10^{-4}	1.19	11.88	9.96
354	3.98	3.053	2.03	14.14	4.48×10^{-2}	5.32×10^{7}	8.43×10^{6}	9.83×10^{-5}	1.19	11.72	9.84
355	3.98	3.241	2.10	14.14	3.98×10^{-2}	6.00×10^{7}	8.43×10^{6}	9.26×10^{-5}	1.19	11.61	9.75
356	3.98	3.443	2.17	14.14	3.53×10^{-2}	6.77×10^{7}	8.44×10^{6}	8.72×10^{-5}	1.19	11.47	9.63
357	3.99	3.645	2.25	14.14	3.16×10^{-2}	7.59×10^{7}	8.46×10^{6}	8.23×10^{-5}	1.20	11.46	9.59
358	3.99	3.847	2.26	14.14	2.83×10^{-2}	8.45×10^{7}	8.45×10^{6}	7.80×10^{-5}	1.19	11.14	9.34
359	4.00	4.048	2.32	14.14	2.57×10^{-2}	9.35×10^{7}	8.48×10^{6}	7.41×10^{-5}	1.20	11.15	9.31
360	3.96	4.250	2.34	14.14	2.30×10^{-2}	1.03×10^{8}	8.40×10^{6}	7.06×10^{-5}	1.19	10.78	9.09
361	4.00	4.453	2.44	14.14	2.12×10^{-2}	1.13×10^{8}	8.47×10^{6}	6.74×10^{-5}	1.20	11.11	9.29
362	4.00	4.655	2.47	14.14	1.94×10^{-2}	1.24×10^{8}	8.48×10^{6}	6.45×10^{-5}	1.20	11.00	9.19
363	4.00	4.858	2.47	14.14	1.78×10^{-2}	1.35×10^{8}	8.48×10^{6}	6.18×10^{-5}	1.20	10.98	9.17
364	4.00	5.061	2.50	14.14	1.64×10^{-2}	1.46×10^{8}	8.47×10^{6}	5.93×10^{-5}	1.20	11.07	9.25

TABLE 6.4: Temperature and heat transport measurements for the annulus with a sloping base, $d(r,\phi)$.

Run No	ΔT K	Ω $rad.sec^{-1}$	ΔT_{BAR} K	Prandtl No	Θ	Taylor No	Rayleigh No	Ekman No	$H_{conductive}$ $watts$	H_{total} $watts$	Nusselt No
365	10.02	0.000	0.23	14.14	∞	0	2.12×10^{7}	∞	3.00	42.87	14.29
366	10.03	0.000	0.23	14.14	∞	0	2.13×10^{7}	∞	3.00	42.95	14.31
367	9.98	0.203	0.33	14.14	2.55×10^{1}	2.34×10^{5}	2.11×10^{7}	1.48×10^{-3}	2.98	42.23	14.15
368	9.98	0.404	0.60	14.14	6.42	9.31×10^{5}	2.11×10^{7}	7.43×10^{-4}	2.98	42.06	14.09
369	9.98	0.605	0.85	14.14	2.86	2.09×10^{6}	2.11×10^{7}	4.96×10^{-4}	2.99	41.99	14.07
370	9.97	0.806	1.09	14.14	1.61	3.71×10^{6}	2.11×10^{7}	3.72×10^{-4}	2.98	41.86	14.03
371	10.00	1.022	1.34	14.14	1.01	5.96×10^{6}	2.12×10^{7}	2.94×10^{-4}	2.99	41.88	14.00
372	9.99	1.224	1.59	14.14	7.00×10^{-1}	8.56×10^{6}	2.12×10^{7}	2.45×10^{-4}	2.99	41.70	13.95
373	9.99	1.426	1.84	14.14	5.16×10^{-1}	1.16×10^{7}	2.12×10^{7}	2.10×10^{-4}	2.99	41.63	13.92
374	9.99	1.628	2.06	14.14	3.96×10^{-1}	1.51×10^{7}	2.12×10^{7}	1.84×10^{-4}	2.99	41.60	13.92
375	10.00	1.830	2.28	14.14	3.14×10^{-1}	1.91×10^{7}	2.12×10^{7}	1.64×10^{-4}	2.99	41.67	13.92
376	10.00	2.031	2.49	14.14	2.54×10^{-1}	2.36×10^{7}	2.12×10^{7}	1.48×10^{-4}	2.99	41.69	13.94
377	10.00	2.233	2.72	14.14	2.10×10^{-1}	2.85×10^{7}	2.12×10^{7}	1.34×10^{-4}	2.99	41.72	13.95
378	10.01	2.435	2.93	14.14	1.77×10^{-1}	3.39×10^{7}	2.12×10^{7}	1.23×10^{-4}	3.00	41.79	13.95
379	10.00	2.636	3.10	14.14	1.51×10^{-1}	3.97×10^{7}	2.12×10^{7}	1.14×10^{-4}	2.99	41.62	13.90
380	10.01	2.839	3.23	14.14	1.30×10^{-1}	4.60×10^{7}	2.12×10^{7}	1.06×10^{-4}	3.00	41.53	13.86
381	10.00	3.039	3.36	14.14	1.14×10^{-1}	5.27×10^{7}	2.12×10^{7}	9.87×10^{-5}	2.99	41.35	13.82
382	10.01	3.241	3.52	14.14	1.00×10^{-1}	6.00×10^{7}	2.12×10^{7}	9.26×10^{-5}	3.00	41.28	13.78
383	10.02	3.443	3.70	14.14	8.87×10^{-2}	6.77×10^{7}	2.12×10^{7}	8.71×10^{-5}	3.00	41.20	13.75
384	10.00	3.645	3.89	14.14	7.90×10^{-2}	7.59×10^{7}	2.12×10^{7}	8.23×10^{-5}	2.99	41.01	13.71
385	9.99	3.847	4.08	14.14	7.09×10^{-2}	8.45×10^{7}	2.12×10^{7}	7.80×10^{-5}	2.99	40.84	13.66
386	10.00	4.048	4.22	14.14	6.41×10^{-2}	9.36×10^{7}	2.12×10^{7}	7.41×10^{-5}	2.99	41.06	13.72
387	10.01	4.250	4.39	14.14	5.82×10^{-2}	1.03×10^{8}	2.12×10^{7}	7.06×10^{-5}	2.99	41.22	13.76
388	9.99	4.453	4.52	14.14	5.29×10^{-2}	1.13×10^{8}	2.12×10^{7}	6.74×10^{-5}	2.99	41.15	13.77
389	10.00	4.655	4.63	14.14	4.84×10^{-2}	1.24×10^{8}	2.12×10^{7}	6.45×10^{-5}	2.99	41.35	13.82
390	10.00	4.858	4.67	14.14	4.45×10^{-2}	1.35×10^{8}	2.12×10^{7}	6.18×10^{-5}	2.99	41.45	13.85
391	9.99	5.060	4.73	14.14	4.10×10^{-2}	1.46×10^{8}	2.12×10^{7}	5.93×10^{-5}	2.99	41.48	13.87

the insulating or conducting barriers and flat bases. The largest value being $\Delta T_B \sim 60\% \Delta T$.

The sloping bases tended to reduce the fluid heat transport measurements compared to the experiments made with flat bases. The most dramatic case being that of the system with $d(r,\phi)$ at $\Delta T \approx 4\ K$, when the Nusselt number fell to around 80% of its non-rotating value at $\Omega \approx 4.0 - 5.0\ rad.sec^{-1}$. This was the only experiment in which eddies were inhibited over the complete range of Ω covered.

6.2 Discussion of results.

Of the experiments with sloping bases, at least one case (the system with $d(r,\phi)$ at $\Delta T \approx 4\ K$) achieved the stated aim of §3.4; namely to suppress eddies so that heat transport measurements in a system without eddies could be compared with heat transport measurements made when eddies were present. While the heat transporting role of the eddies is more fully discussed in §6.2.3 below, comparison of *Figure 6.8(a)* with *Figures 3.11(a)* and *3.17(a)* suggests that eddies play a significant role in heat advection, because the heat transport in the system with no eddies drops off at high Ω, but does not in the system where eddies were present.

The following discussion assumes that the fluid motions in the systems with sloping bases were basically the same as those observed in the systems with flat bases, as no velocity measurements were made in the systems with sloping bases.

The use of sloping bases in these experiments means that equations (3.16) and (3.22) no longer describe the η and ζ - circulations correctly, and that new expressions will have to be derived from equations (3.15) and (3.21).

The following sections deal in turn with heat advection by each of the three significant processes occuring in the fluid; the η-circulation, (§6.2.1) the ζ-circulation

(§6.2.2) and eddies (§6.2.3).

6.2.1 Heat transport by the η-circulation.

If the flow with a sloping base is suitably similar to that observed with a flat base then $H_\eta(\bar{r};\phi,z,t)$ is given by equation (3.15). As the surface $\mathcal{S}$ mentioned in §3.2.2 is at constant radius, $r = \bar{r}$, the only difference between the sloping bases $d(\phi)$ and $d(r,\phi)$ is that the dependence of $a(\bar{r};\phi)$ (see equation (3.3)) on ϕ will be slightly different in each case.

Comparison of equations (3.15) and (3.16) shows that

$$H_\eta(\bar{r}, a \neq 0; \phi, z, t) \approx H_\eta(\bar{r}, a = 0; t) + H_\eta^{slope}(\bar{r}, z = 0; \phi, t), \qquad (6.1)$$

where $H_\eta(\bar{r}, a = 0; t)$ is given by equation (3.16) and

$$\begin{aligned} &H_\eta^{slope}(\bar{r}, z = 0; \phi, t) \approx \\ &\frac{\bar{\rho}\bar{C}_p g\alpha \Delta T_\phi(\bar{r}, z = 0; t)}{4\Omega\pi} \int_{\phi_0}^{\phi_1} \left[\frac{\Delta T_\phi(\bar{r}, z = 0; t)}{4\pi} \phi a(d-a) \right. \\ &\left. + \frac{\Delta T_z(\bar{r}, \phi = 0; t)}{3d} \left(-\frac{3ad^2}{4} + \frac{3a^2 d}{2} - a^3 \right) + \frac{T'(\bar{r}, z = 0; \phi, t)}{2} a(d-a) \right] d\phi. \end{aligned} \qquad (6.2)$$

Since the annulus has a sloping base, $a(\bar{r};\phi) \neq 0$. The bases both had a linear slope with ϕ, so that $a(\bar{r};\phi) = b\phi + c(\bar{r})$. Substituting for $a(\bar{r},\phi)$ and integrating between the limits given in (3.3) gives

$$\begin{aligned} &H_\eta^{slope}(\bar{r}, z = 0; \phi, t) \approx \\ &\frac{\bar{\rho}\bar{C}_p g\alpha \Delta T_\phi(\bar{r}, z = 0; t)}{4\Omega\pi} \left\{ \frac{\Delta T_\phi(\bar{r}, z = 0; t)}{4\pi} b(d - 2c) \frac{2(\pi-\epsilon)^3}{3} \right. \\ &+ \frac{\Delta T_z(\bar{r}, \phi = 0; t)}{3d} \left[-\frac{3cd^2}{4} 2(\pi - \epsilon) + \frac{3d}{2} \left(b^2 \frac{2(\pi-\epsilon)^3}{3} + c^2 2(\pi - \epsilon) \right) \right. \\ &\left. -3b^2 c \frac{2(\pi-\epsilon)^3}{3} - c^3 2(\pi - \epsilon) \right] \\ &\left. + \int_{\phi_0}^{\phi_1} \frac{T'(\bar{r}, z = 0; \phi, t)}{2} a(\bar{r};\phi) \left(d - a(\bar{r};\phi) \right) d\phi \right\}. \end{aligned}$$

Since the angular half-width of the barrier, $\epsilon \ll \pi$ it can be neglected, so that

$$H_\eta^{slope}(\bar{r}, z=0;\phi,t) \approx \frac{\bar{\rho}\bar{C}_p g\alpha \Delta T_\phi(\bar{r}, z=0;t)\Delta T_z(\bar{r},\phi=0;t)d^2}{24\Omega}\left\{\frac{\Delta T_\phi(\bar{r}, z=0;t)}{\Delta T_z(\bar{r},\phi=0;t)d^2}b(d-2c)\pi + \frac{1}{d^2}\left[-3cd+2b^2\pi^2+6c^2-\frac{4b^2c\pi^2}{d}-\frac{4c^3}{d}\right] + \frac{3}{\Delta T_z(\bar{r},\phi=0;t)\pi d^2}\int_{\phi_0}^{\phi_1} T'(\bar{r}, z=0;\phi,t)a(\bar{r};\phi)(d-a(\bar{r};\phi))d\phi\right\}. \quad (6.3)$$

$H_\eta(\bar{r}, a\neq 0;\phi,z,t)$ (see equation (6.1)) is plotted in *Figures 6.12* and *6.13*[1].

If $H_\zeta(\bar{r}, a\neq 0;\phi,z,t)$ and $H'(\bar{r};\phi,z,t)$ can be neglected at small values of Ω (see §3.2.4), then for the systems with sloping bases,

$$H_{adv}(\bar{r};\phi,z,t) \approx H_\eta(\bar{r}, a\neq 0;\phi,z,t).$$

If this is the case, then using equation (6.1),

$$H_{adv}(\bar{r}, a\neq 0;t) \approx H_\eta(\bar{r}, a=0;t) + H_\eta^{slope}(\bar{r}, z=0;\phi,t).$$

Hence it is possible to define A_*^{-1} by equation (3.17), so that

$$A_*^{-1} \approx \frac{24\Omega}{\bar{\rho}\bar{C}_p g\alpha\Delta T_B \Delta T_z(\bar{r},\phi=0;t)d^2}\left(H_\eta(\bar{r}, a=0;t) + H_\eta^{slope}(\bar{r}, z=0;\phi,t)\right).$$

Thus, using $\Delta T_\phi = \Delta T_B$ and $\Delta T_z \approx \Delta T$,

$$A_*^{-1} \approx 1 + \frac{\Delta T_B}{\Delta T d^2}b\pi(d-2c) - \frac{3c}{d} + \frac{2b^2\pi^2}{d^2} + \frac{6c^2}{d^2} - \frac{4b^2c\pi^2}{d^3} - \frac{4c^3}{d^3} + \frac{3}{\Delta T\pi d^2}\int_{\phi_0}^{\phi_1} T'(\bar{r}, z=0;\phi,t)a(\bar{r};\phi)(d-a(\bar{r};\phi))d\phi. \quad (6.4)$$

Notice that when $b=c=0$, *i.e.* $a(\bar{r};\phi)=0$, or when $b,c \ll d$, then $A_*^{-1}\approx 1$. The values of b and c are determined by the dimensions of the base and are given in *Table 6.5.*

[1] $\int T'a(d-a)d\phi$ was calculated as follows: $\int_{\phi_0}^{\phi_1} T'a(d-a)d\phi \approx \Sigma_{i=1}^{32} T_i' a_i(d-a_i)\delta\phi$, where $a_i = a(\bar{r};\phi_i)$, and T_i', ϕ_i and $\delta\phi$ are given in §3.2.5.

Type of base	b	$c(\bar{r})$
$d(\phi)$	$1.90/\pi$ $cm.rad^{-1}$	3.10 cm
$d(\bar{r};\phi)$	$0.65/\pi$ $cm.rad^{-1}$	3.20 cm

TABLE 6.5: Coefficient values for the two bases used in the variable depth experiments. For b and c see the main text.

Calculation using equation (6.4) shows that the terms in ΔT_B and T' contribute very little (less than 0.028 and 0.006 respectively) to A_*^{-1}, so that A_*^{-1} is found to be virtually independent of Ω with a value of ~ 0.6 for both sloping bases. Values of A_*^{-1} from equation (3.17) are plotted in *Figure 6.9.* It can be seen that the values of A_*^{-1} tend to be of the order of, but somewhat smaller than, 0.6 at smaller values of Ω (which is when the best agreement would be expected, see §3.2.4), having a value of around 0.4 in (a) and (b). If this discrepancy is attributed to the error caused by estimating ΔT_z by ΔT, then it suggests that in the sloping base experiments $\Delta T_z \sim \frac{2}{3}\Delta T$. Accordingly $\Delta T_z = \frac{2}{3}\Delta T$ has been used in the following analysis for the $d(\phi)$ sloping base results.

It is harder to apply a similar interpretation to the values of A_*^{-1} calculated for the $d(r,\phi)$ sloping base ((c) and (d)) as they rise more gradually over the whole range of Ω. However equation (3.17) shows that A_*^{-1} is proportional to H_{adv}, thus the rise in A_*^{-1} might be expected to be due to one of the three heat advection processes explored so far (the η-circulation, the ζ-circulation, or eddies). As there were no eddies present for the results in (c), and as the η-circulation is characterised by constant A_*^{-1} the increase may be due to the ζ-circulation. Thus A_*^{-1} should only be expected to be close to 0.6 at values of Ω small enough for the heat advection of the ζ-circulation to be unimportant, but not so close to $\Omega = 0$ that the azimuthal geostrophic balance is doubtful. At $\Omega \approx 1.0$ $rad.sec^{-1}$, A_*^{-1} has a value of about 0.32. The ratio of this value to 0.6, suggests that for the $d(r,\phi)$ results, a good estimate of ΔT_z may be $0.53\Delta T$. Thus $\Delta T_z = 0.53\Delta T$ has been used in the following analysis for the $d(r,\phi)$ results.

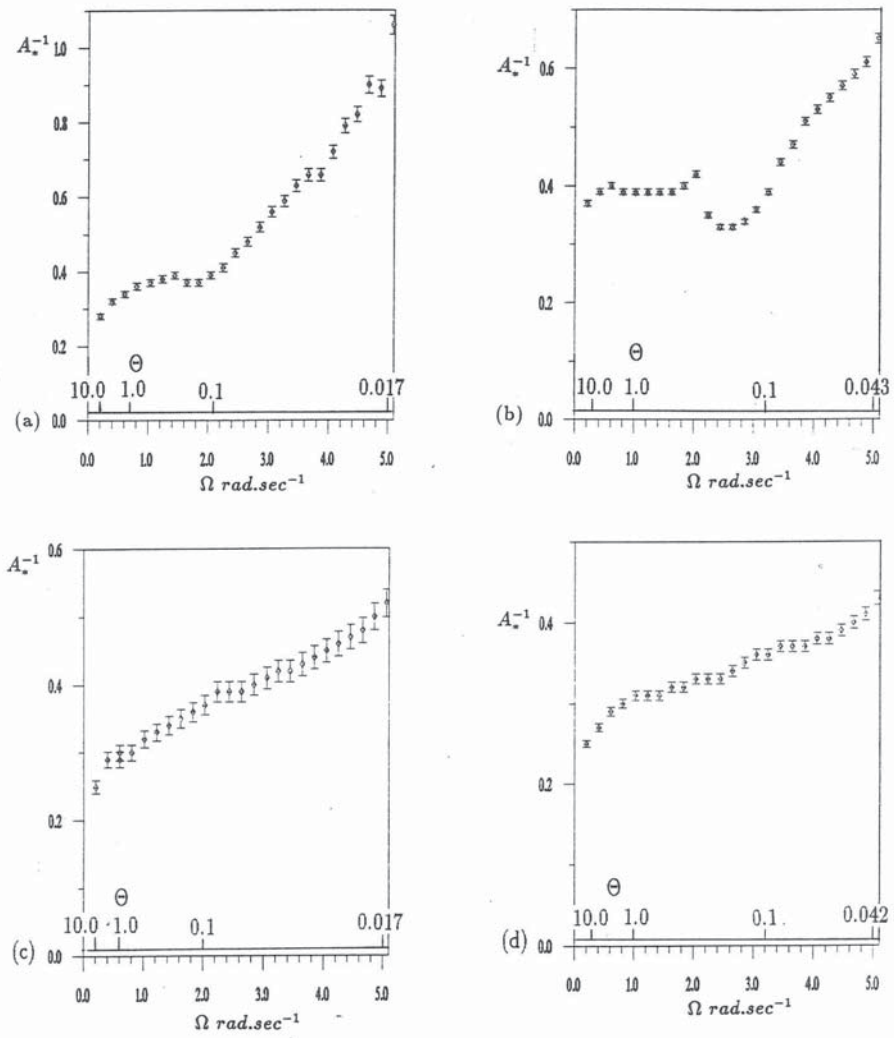

FIGURE 6.9: Plots of the dimensionless quantity A_*^{-1} (given in equation (3.17)) against Ω, for (a), (b) the system with $d = d(\phi)$ and (c), (d) the system with $d = d(r, \phi)$. (a), (c) $\Delta T \approx 4\ K$, and (b), (d) $\Delta T \approx 10\ K$. In all cases $A_*^{-1} \sim 0.6$. In (a), (b) there is a marked increase in A_*^{-1} at high Ω, while in (c), (d) A_*^{-1} remains more nearly constant.

It is interesting to note that these estimates of ΔT_z seem to indicate a qualitative result suggested by equation (4.1), namely that for fully blocked systems larger values of ΔT_ϕ appear to be associated with smaller values of ΔT_z, for a given Ω and ΔT. It is also quite possible that ΔT_z may vary with Ω.

The quantity $Y(\bar{r}, a \neq 0; \Omega, t) \approx \Delta T_B$ (see §3.2.4) can still be plotted using equation (3.20) with $H_{adv}(\bar{r}, a \neq 0; t)$ instead of $H_{adv}(\bar{r}, a = 0; t)$, and equations (3.18) and (3.19). In this case $\bar{d}$ the average depth of the annulus has been used instead of d. Y is shown plotted against ΔT_B in *Figures 6.10* and *6.11*, and it can be seen that for values of $A \approx 1.7$ and $R \sim 1\ cm$, $Y \approx \Delta T_B$.

6.2.2 Heat transport by the ζ-circulation.

If the flow with a sloping base is suitably similar to that observed with a flat base, then $H_\zeta(\bar{r}; \phi, z, t)$ is given by equation (3.21). Proceeding in the same manner as in §6.2.1, comparison of equations (3.21) and (3.22) shows that

$$H_\zeta(\bar{r}, a \neq 0; \phi, z, t) \approx H_\zeta(\bar{r}, a = 0; \phi, t) + H_\zeta^{slope}(\bar{r}, z = 0; \phi, t), \qquad (6.5)$$

where

$$H_\zeta^{slope}(\bar{r}, z = 0; \phi, t) \approx \frac{\bar{\rho}\bar{C}_p \Delta u_\phi(\bar{r}, z = 0; t)}{2\pi} \int_{\phi_0}^{\phi_1} a(\bar{r}; \phi) \left[-\frac{\Delta T_\phi(\bar{r}, z = 0; t)}{2\pi} \phi^2 + \frac{\Delta T_z(\bar{r}, \phi = 0; t)}{2d} \phi(d - a(\bar{r}, \phi)) - T'(\bar{r}, z = 0; \phi, t)\phi \right] \bar{r} d\phi. \qquad (6.6)$$

The sloping bases mean that $a(\bar{r}, \phi) = b\phi + c(\bar{r})$, and substitution and integration between the limits given in (3.3), neglecting the angular half-width of the barrier ϵ, gives

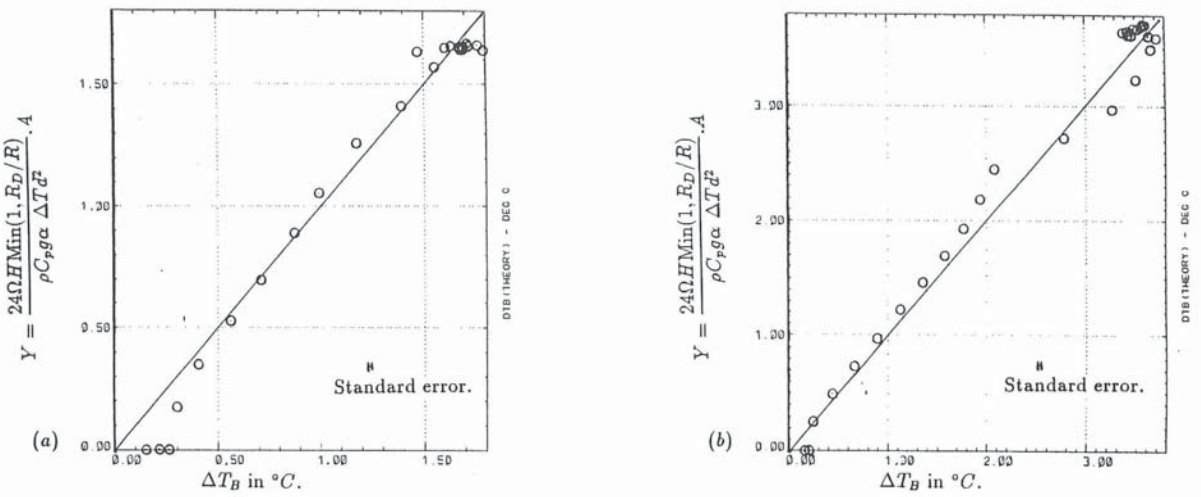

FIGURE 6.10: Plots of the quantity Y against ΔT_B for the system with $d(\phi)$. (a) $\Delta T \approx 4\ K$, $A = 1.68$, $R = 0.93\ cm$, (b) $\Delta T \approx 10\ K$, $A = 1.69$, $R = 0.97\ cm$. In both cases the results fall quite closely onto a straight line of gradient unity, indicating that $\Delta T_B \approx Y$.

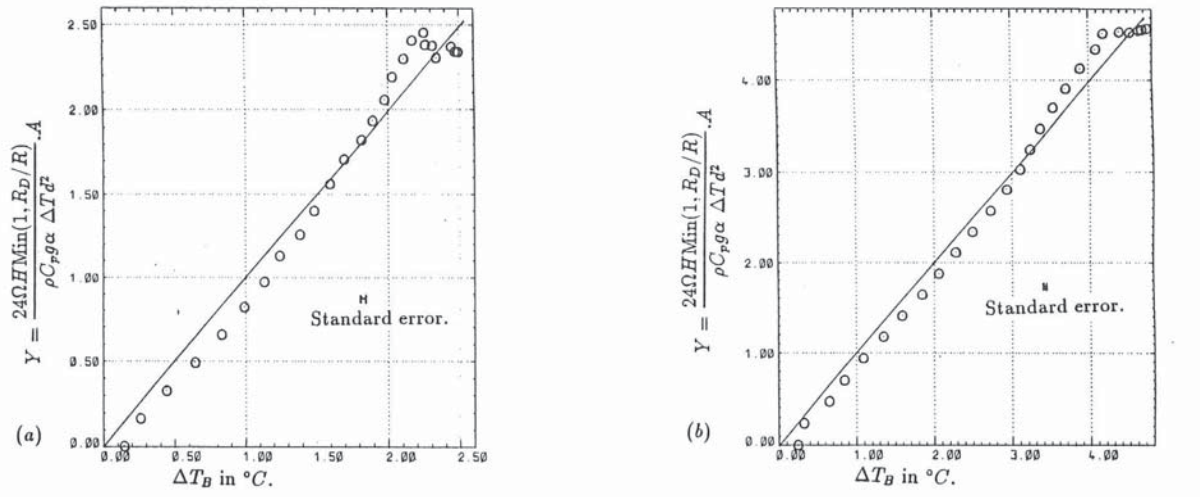

FIGURE 6.11: Plots of the quantity Y against ΔT_B for the system with $d(r, \phi)$. (a) $\Delta T \approx 4\ K$, $A = 1.50$, $R = 0.50\ cm$, (b) $\Delta T \approx 10\ K$, $A = 1.65$, $R = 0.70\ cm$. In both cases the results fall quite closely onto a straight line of gradient unity, indicating that $\Delta T_B \approx Y$.

$$H_\zeta^{slope}(\bar{r}, z=0; \phi, t) \approx \frac{\bar{\rho}\bar{C}_p \Delta u_\phi(\bar{r}, z=0; t)\bar{r}}{2\pi} \left\{ \left[-\frac{\Delta T_\phi(\bar{r}, z=0; t)}{\pi} c + \frac{\Delta T_x(\bar{r}, \phi=0; t)}{d} b(d-2c) \right] \frac{\pi^3}{3} - \int_{\phi_0}^{\phi_1} T'(\bar{r}, z=0; \phi, t) a(\bar{r}; \phi) \phi d\phi \right\}. \quad (6.7)$$

Δu_ϕ is given in §3.2.5. The value of $H_\zeta(a=0) + H_\zeta^{slope}$ from equations (3.23) and (6.7) is plotted in *Figures 6.12* and *6.13*[2].

6.2.3 Heat transport by eddies.

Previous calculations indicated that the eddies were quite capable of advecting significant quantites of heat (§3.2.6 and §4.2.2). The purpose of the sloping bases was to attempt to inhibit the formation of eddies so that heat advection measurements without eddies could be compared with the heat advection contributions calculated for the η and ζ-circulations. Thus it is the results with the $d(r, \phi)$ base at $\Delta T \approx 4\ K$ which are of most interest, because for that case no eddies were seen over the entire range of Ω used. Also the previous calculations had shown that the values of H_0' were very small (see *Figures 3.17* and *4.16*), so it has been neglected.

The $d(r, \phi), \Delta T \approx 4\ K$ results are given in *Figure 6.13(a)*. It can be seen that over the full range of Ω, the sum of the heat advection contributions from the η and ζ-circulations gave much better agreement with the experimentally measured heat advection, H_{adv}, than any of the other systems at $\Delta T \approx 4\ K$.

[2] $\int T' a \phi d\phi$ was calculated as follows: $\int_{\phi_0}^{\phi_1} T' a \phi d\phi \approx \Sigma_{i=1}^{32} T_i' a_i \phi_i \delta\phi$, where the terms are the same as those in §6.2.1.

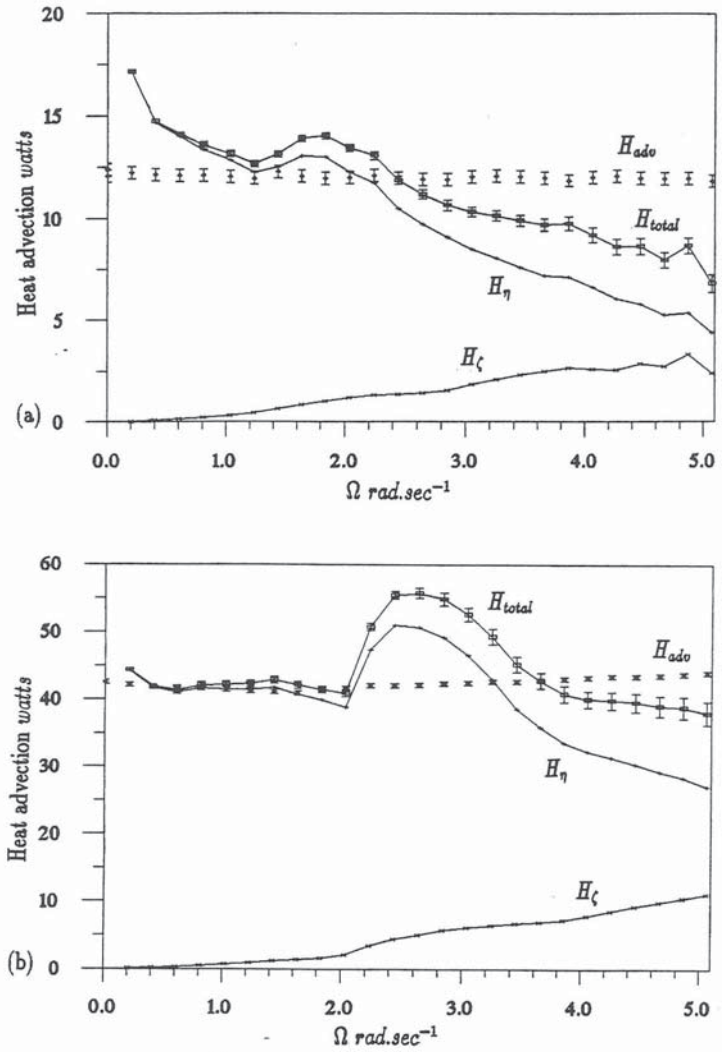

FIGURE 6.12: Plots showing the heat transport contributions for the insulating barrier with sloping base, $d(\phi)$. Heat transport contributions have been calculated for; the η-circulation, $H_\eta(a \neq 0)$, using equations (3.16) and (6.3); and the ζ-circulation, $H_\zeta(a \neq 0)$, using equations (3.23) and (6.7). $\frac{2}{3}\Delta T$ was used as the estimate of ΔT_x. $H_{total} = H_\eta + H_\zeta$. Experimental measurements of the advective heat transport, H_{adv} are shown for comparison. (a) $\Delta T \approx 4\ K$, (b) $\Delta T \approx 10\ K$. The lines serve only as a guide to the eye.

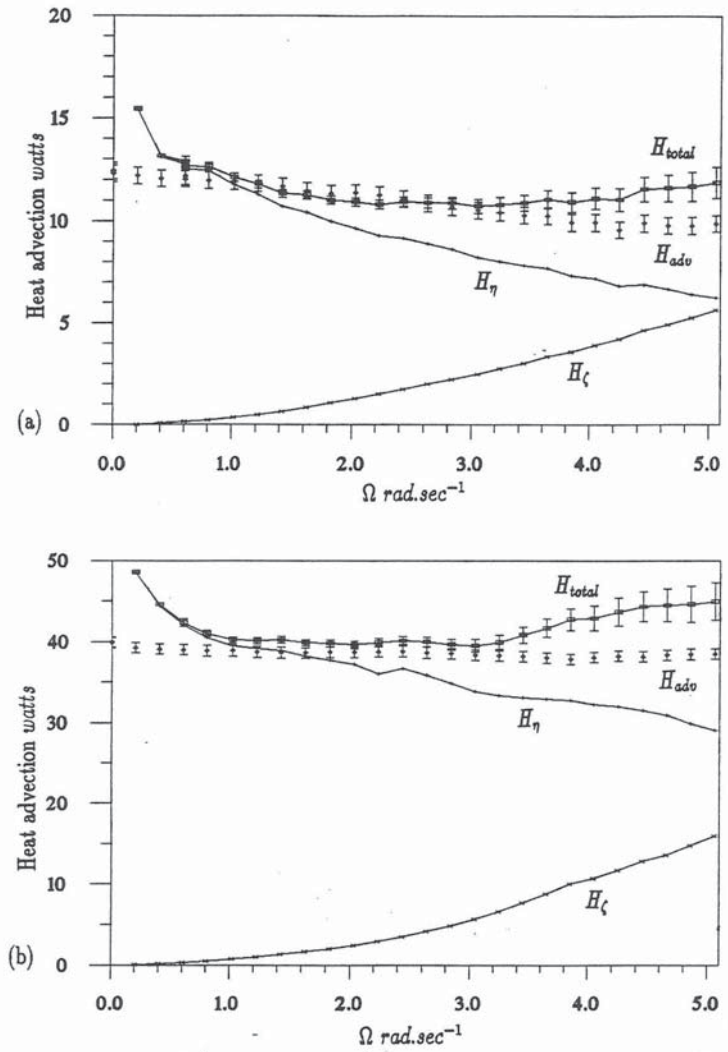

FIGURE 6.13: Plots showing the heat transport contributions for the insulating barrier with sloping base, $d(r,\phi)$. Heat transport contributions have been calculated for; the η-circulation, $H_\eta(a \neq 0)$, using equations (3.16) and (6.3); and the ζ-circulation, $H_\zeta(a \neq 0)$, using equations (3.23) and (6.7).ΔT_s was estimated as $0.53 \times \Delta T$. $H_{total} = H_\eta + H_\zeta$. Experimental measurements of the advective heat transport, H_{adv} are shown for comparison. (a) $\Delta T \approx 4\ K$, (b) $\Delta T \approx 10\ K$. The lines serve only as a guide to the eye.

This suggests that the total advective heat transport is well described by the η and ζ-circulations (§§3.2.3, 3.2.5, 6.2.1 and 6.2.2) when there are no eddies present. This in turn implies that the discrepancies seen at high Ω in *Figures 3.17(a), 4.16(a)* and *6.12(a)* arise because of heat advection by eddies.

Interestingly, *Figure 6.13(b)* shows almost as good agreement between the theory and measurements as there is in (a), even though eddies were seen in the $d(r,\phi), \Delta T \approx 10\ K$ measurements. However this result is broadly in agreement with the other experiments, where better agreement at high Ω was generally seen at $\Delta T \approx 10\ K$ than at $4\ K$ (*Figures 3.17(b), 4.16(b)* and *6.12(b)*). This may also be because the $d(r,\phi)$ sloping base suppresses other effects not described in the theory. A similar phenomenon may be occuring at small Ω for the $d(\phi)$ results (*Figure 6.12*) where better agreement is seen than for the experiments with a flat base.

6.3 Conclusions.

In chapters 3 and 4 it was established that at low to medium Ω, the advective heat transport was quite well described by the theory for the η and ζ-circulations. The largest outstanding discrepancy occurred at high Ω, where the heat advection measurements were not fully accounted for by the η and ζ-circulations (see *Figure 3.17*).

At $\Delta T \approx 4\ K$ the $d(r,\phi)$ sloping base suppressed the formation of eddies, and the measurements of total heat advection were found to agree quite closely with that predicted by the η and ζ-circulations. This strongly suggests that the discrepancy seen at high Ω in *Figure 3.17(a)* was due to heat advection by eddies. The small difference that exists between $H_{total}(a \neq 0)$ and H_{adv} in *Figure 6.13(a)* may quite likely be because the velocity shear of the ζ-circulation, Δu_ϕ was overestimated by using the velocity measurements for the flat base experiments

(§3.2.5).

In general the results with the sloping bases, *Figures 6.12* and *6.13* show better agreement with the theory at smaller values of Ω than the measurements with flat bases. This may be because the sloping bases tend to reduce the importance of factors other than eddies, which were not well represented in the theory. In particular the dependence of $\partial T/\partial\phi$ on z, and of ΔT_z on Ω may be significant. Also the non-linear temperature field was approximated by $T'(\bar{r}, z = 0; \phi, t)$ in equation (3.5), so that it could be calculated from the thermocouple ring data. The fact that *Figures 6.12* and *6.13* show quite good agreement at $\Omega \approx 0.6 \rightarrow 2.0$ $rad.sec^{-1}$ suggests that the disagreements in *Figure 3.17* at those rotation rates do not arise because of a breakdown in azimuthal geostrophic balance, but for some other reason.

The fact that the sloping bases suppressed the formation of the eddies seen in the fully blocked annulus system provides some evidence as to the nature of the eddies. Regardless of the calculations involving the η and ζ-circulations above, the results with the $d(r, \phi)$ sloping base demonstrate two important points; (i) a suitably shaped sloping base can suppress the formation of eddies in the fully blocked annulus system, and (ii) comparison between *Figures 3.11* and *6.8* shows that the eddies transport heat. The work of *Mason (1975)* and *Hide and Mason (1975)* shows that these two characteristics are shared by baroclinic wave flows. Considering the manner in which sloping bases affect the flows (see the start of this chapter for a discussion) the fact that the eddies were suppressed by the sloping bases provides possibly very significant evidence that these eddies are baroclinic in nature.

6.4 Further investigations.

Since ΔT_z was not measured it has been necessary to estimate it, either as ΔT (in the first instance), or from the plots of A_*^{-1}. Apart from the significant role ΔT_z plays in the formulation for heat advection by the η-circulation, the results seem to suggest that the relationship of ΔT_z to ΔT_ϕ (or ΔT_B) might prove quite interesting (equation (4.1) and §6.2.1). Suitable measurements of temperature against height might also give an indication of how linear the vertical temperature profile is. T' could then possibly be integrated numerically over both ϕ and z. If a series of measurements was made with an array of thermocouples in a (ϕ, z)-plane this would also allow the dependence of $\partial T/\partial\phi$ on z to be discovered.

§6.3 suggests that the ζ-circulation might be overestimated in §6.2.2 and *Figures 6.12* and *6.13*. Suitable velocity measurements might give a more accurate estimation of Δu_ϕ.